iScience

Article

Elucidation of the suppression of photoinduced segregation in 2D mixed halide, $A_2PbI_2Br_2$: Critical role of A_2PbBr_4 photostability

Graphical abstract

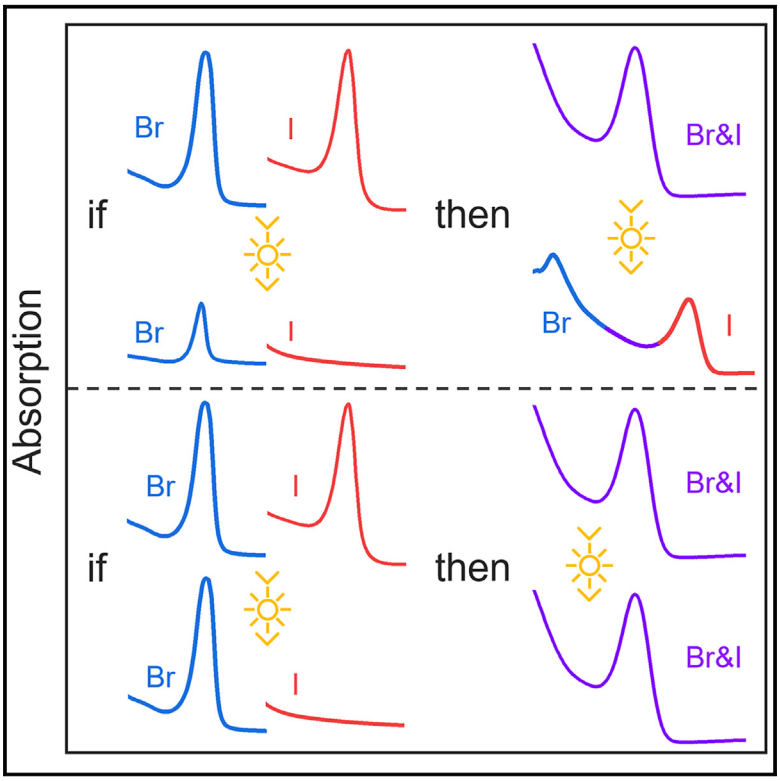

Highlights

- Photoinduced halide segregation (PHS) in 2D perovskites is spacer cation dependent
- Photooxidative degradation of 2D perovskites is also spacer cation dependent
- PHS and photooxidative degradation occur due to photo/electrochemical redox reactions
- PHS is suppressed by reduced spacer vacancy formation when photostable phase exists

Authors

Zhilin Ren, Zhengtian Yuan, Juraj Ovčar, ..., Ivor Lončarić, Jasminka Popović, Aleksandra B. Djurišić

Correspondence

ivor.loncaric@irb.hr (I.L.), jasminka.popovic@irb.hr (J.P.), dalek@hku.hk (A.B.D.)

In brief

Natural sciences; Applied sciences; Materials science

Ren et al., 2025, iScience *28*, 112154
April 18, 2025
https://doi.org/10.1016/j.isci.2025.112154

CellPress

iScience

CellPress
OPEN ACCESS

Article

Elucidation of the suppression of photoinduced segregation in 2D mixed halide, $A_2PbI_2Br_2$: Critical role of A_2PbBr_4 photostability

Zhilin Ren,[1,7] Zhengtian Yuan,[1,7] Juraj Ovčar,[2,8] Tik Lun Leung,[1,4,5,8] Yanling He,[6] Anita W.Y. Ho-Baillie,[4,5] Ivor Lončarić,[3,*] Jasminka Popović,[3,*] and Aleksandra B. Djurišić[1,9,*]

[1]Department of Physics, The University of Hong Kong, Pokfulam, Hong Kong SAR
[2]CNR-IOM, Via Bonomea 265, 34136 Trieste, Italy
[3]Ruđer Bošković Institute, Bijenička 54, 10000 Zagreb, Croatia
[4]School of Physics, The University of Sydney, Sydney, NSW 2006, Australia
[5]Sydney Nano, The University of Sydney, Sydney, NSW 2006, Australia
[6]Material characterization and preparation facility, The Hong Kong University of Science and Technology (Guangzhou), No.1 Duxue Road, Dongchong Town, Nansha District, Guangzhou, Guangdong Province, China
[7]These authors contributed equally
[8]These authors contributed equally
[9]Lead contact
*Correspondence: ivor.loncaric@irb.hr (I.L.), jasminka.popovic@irb.hr (J.P.), dalek@hku.hk (A.B.D.)
https://doi.org/10.1016/j.isci.2025.112154

SUMMARY

2D lead halide perovskites are used to improve device operational stability due to increased environmental stability and reduced ion migration compared to 3D perovskites. However, the relationship between the 2D perovskite stability under illumination and spacer cation is still not well understood. Thus, we examine photoinduced halide segregation (PHS) in different 2D mixed-halide perovskites and show that PHS is suppressed in the materials which have photostable bromide halide phase. As the spacer cations provide the barrier to ion migration in 2D perovskites, PHS would be facilitated by the loss of spacer cations through their interactions with various mobile oxidized halide species, resulting in organic ammonium deprotonation and spacer cation vacancy formation. The existence of a photostable A_2PbBr_4 phase, which does not exhibit spacer cation loss, results in the suppression of PHS in 2D mixed halide perovskites due to reduced spacer vacancy formation and consequently reduced halide ion migration under illumination.

INTRODUCTION

2D lead halide perovskites have been commonly proposed to improve the stability of 3D lead halide perovskites $APbX_3$, where A is a small organic cation or Cs^+ and X is halide anion.[1–6] These materials can be described with a formula $C_2A_{n-1}Pb_nX_{3n+1}$ for commonly used Ruddlesden-Popper perovskites, where C is the bulky organic spacer cation which separates the perovskite octahedral layers, while n is the number of layers.[1] They are commonly assumed to exhibit increased stability when exposed to humidity and/or elevated temperature, and to suppress ion migration,[1,2,5] and they have resulted in device stability improvements both for quasi-2D ($n > 1$) and 3D/2D ($n = 1$) perovskites.[4–6] The suppression of ion migration in 2D perovskites is particularly interesting for improving device operational stability, and it is commonly attributed to increased barrier to out-of-plane ion migration[1,2,5] caused by the presence of bulky spacer cations between the layers,[1,5] and reduced concentration of halide and small cation vacancies for in-plane ion migration.[5] These factors also suppress photoinduced halide segregation (PHS),[5] although in this case preferential distribution of Br and I sites within 2D perovskite could also play a role in the suppression[5,7] since I^- and Br^- exhibit different preferences for occupation of axial and equatorial sites.[7,8]

To date, PHS and/or ion migration have been investigated in different 2D and/or quasi-2D perovskites both experimentally[3,9–21] and theoretically.[22,23] In general, halide diffusion was more significant in quasi-2D ($n > 1$) than 2D ($n = 1$) materials,[12,16,17,20,21] but there is very pronounced difference in behavior of 2D perovskites with different spacer cations. Significant PHS in 2D perovskites has been reported for some spacer cations,[9–11,19] while for others, such as phenethylammonium (PEA),[10,11,16,20] negligible photoinduced segregation is observed over similar timescales. For some spacer cations, such as commonly studied butylammonium (BA), not only there was a significant photoinduced segregation in $BA_2PbI_2Br_2$ but also expulsion of both I^- and Br^- into the solution was observed under illumination and bias.[9,24] The instability of some 2D materials under illumination,[9] as well as the evidence of migration of both anions and cations (including bulky spacer cations) in this class of materials,[24–27] has resulted in questioning of the use of 3D/2D approach to stability improvements in the perovskite devices.[9] It

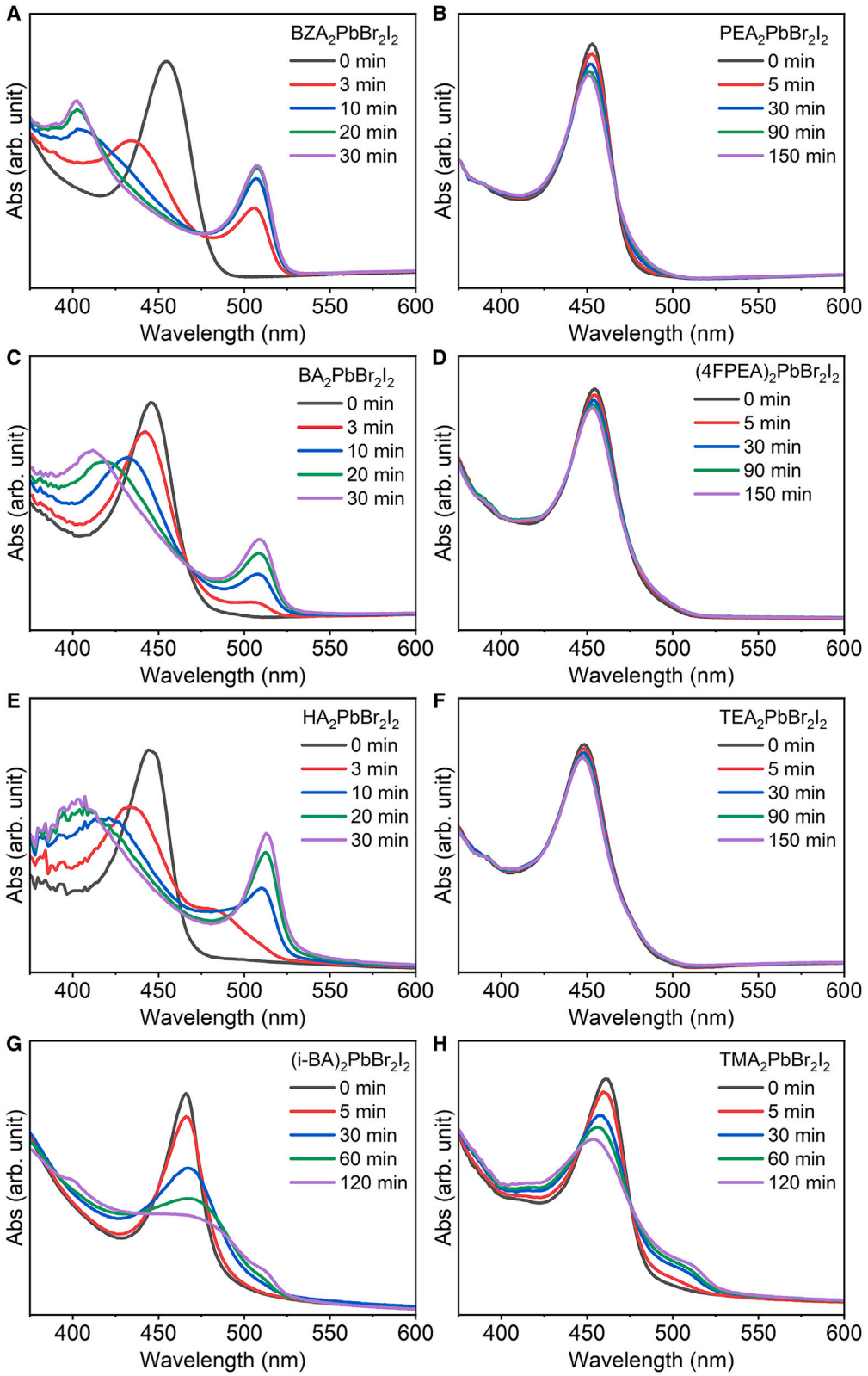

(legend on next page)

is therefore imperative to improve our understanding of ion migration and/or photoinduced segregation in 2D perovskites to facilitate rational selection of 2D capping layers for improved device stability.

Efforts have been made to elucidate which properties of the spacer cation are responsible for the suppression of halide ion migration.[3,12,14,16,20,22,23,25] These studies generally agree that bulkier π-conjugated spacers can inhibit halide diffusion more compared to short chain aliphatic spacers.[3,12] Increased stability and reduced ion transport were linked to increased length of the spacer cation,[22] increased interactions between spacer cations,[25] and increased lattice rigidity,[12,14] as bulkier and stiffer cations would result in higher energy for halide vacancy formation, which in turn would result in slower halide diffusion.[14] In contrast, increased ligand polarization was proposed to increase ion transport.[22] In addition, the suppression of halide diffusion was also attributed to non-binomial halide distribution[20] and to reduced charge separation and consequently lower halide mobility[16] in 2D perovskites. Computational attempts to explain ion transport in 2D perovskites include diffusion coefficient calculations (calculated analytically and estimated from kinetic Monte Carlo simulations),[3] thermodynamic calculations,[23] and molecular dynamic simulations.[12,22] However, these models do not take into account redox reactions which occur in halide perovskite materials (both 3D and 2D) under illumination. Furthermore, the number of spacer cations considered in the same study (to eliminate variations due to differences in methods among different studies) is much smaller for experimental (up to four)[3] compared to computational (up to seven)[22] studies, which hinders comparisons between experiments and theoretical predictions. Consequently, the mechanism of halide segregation as well as cation migration in 2D perovskites is still not well understood.[25]

It should be noted that PHS phenomenon has been investigated more comprehensively in 3D perovskites[28–40] compared to 2D perovskites. Various explanations have been proposed to clarify the PHS in 3D perovskites,[28–38] including processes involving defects/charge trapping through various mechanisms,[28–31] polaron formation,[37,38] and photogenerated carrier funneling.[32–34,36] Consequently, different mathematical models of driving forces for halide segregation, namely miscibility gap model (internal lattice strain), polaron-assisted lattice strain, and photocarrier energy model were proposed.[35] In recent years, however, the role of photo/electrochemical redox reactions in PHS and ion migration has been gaining more recognition.[39–41] It should be noted that this explanation is fully consistent with the recognized roles of defects in the process,[28] as defects are generated in the electrochemical redox reactions, as well as I_2-induced photoinstability,[30,31] as I_2 is a product of I^- oxidation by photogenerated holes.[35,40] Due to differences in redox properties (iodide is more readily oxidized than bromide and the oxidation forms highly mobile oxidized species)[40,41] and bandgaps (charge carrier funneling to lower bandgap iodide-rich domains occurs),[40] the photo/electrochemical redox processes offer a possibility to provide a unified explanation of different experimental observations under illumination and/or bias. The important difference compared to other models is that photo/electrochemical redox reactions take into account continuous generation and annihilation of defects under illumination or bias, and the fact that oxidized halide species is not restricted to vacancy hopping mode of transport as oxidized halide species, such as interstitial iodide and I_2, are highly mobile.[41] Consequently, these processes are expected to play an important role in all types of perovskite materials, and need to be considered when investigating PHS in 2D perovskites.

RESULTS AND DISCUSSION

Here, we examined PHS in 2D lead halide perovskites under simulated solar illumination using *in-situ* absorption measurements, as shown in Figure 1. In addition to commonly studied BA-based and PEA-based perovskites, we considered 6 additional spacer cations, namely benzylammonium (BZA), hexylammonium (HA), 2-thiophenmethylammonium (TMA), 2-thiophenethylammonium (TEA), 4-fluoro-phenethylammonium (4FPEA), and *iso*-butylammonium (i-BA). We can observe that for some spacer cations, 2D perovskite readily segregates, while others exhibit good photostability. The obtained results for the two commonly studied 2D perovskites, $BA_2PbI_2Br_2$ and $PEA_2PbI_2Br_2$, are in agreement with previous reports of significant segregation for BA[9–11] and negligible segregation for PEA,[10,11,20] as well as the report of one magnitude slower halide ion mixing for PEA compared to BA.[14] It is also interesting to note that slower PEA cation migration compared to BA cation migration was also observed.[24] Perovskite with TEA spacer exhibited similar behavior to PEA, in agreement with similarity in ion transport for these two spacers, which exhibited much slower ion transport compared to BA-based perovskites in lateral diffusion experiments.[12] Thus, reported trends in the literature, with BA exhibiting significant PHS and PEA and TEA having improved photostability[9–11,14,20] are in excellent agreement with our results. Nevertheless, it should be noted that direct comparisons between different studies of PHS could be affected by light source and light intensity used, as well as the film quality (grain size, crystallinity, and native defect concentrations). However, when materials studied exhibit such pronounced difference in behavior, as observed for BA and PEA, it is expected that the same trends are observed across different reports and this is indeed the case. One significant observation from these experiments is that while significant ion transport and consequently PHS is indeed observed for short aliphatic chain spacers in agreement with expectations,[3,15] we observe varied response in π-conjugated spacers, which are expected to exhibit suppression of ion transport.[15] From a previous experimental observation of PHS in 2D perovskite with phenylpropylammonium (PPA) spacer,[19] it is obvious that perovskites with π-conjugated spacers can indeed segregate, but the mechanisms responsible for fast segregation for BZA and suppressed segregation for PEA and 4FPEA are not fully clear.

Figure 1. *In-situ* absorption spectra of 2D mixed halide perovskite under illumination

In-situ absorption spectra recorded at different times during the photoinduced segregation under 100 mW/cm^2 simulated solar illumination for mixed halide perovskite $A_2PbBr_2I_2$, where A denotes the following spacer cations (A) BZA (B) PEA (C) BA (D) 4FPEA (E) HA (F) TEA (G) i-BA (H) TMA.

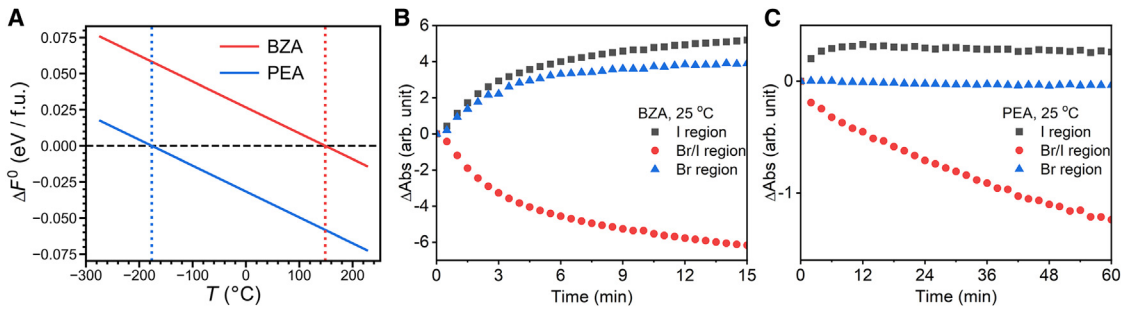

Figure 2. Helmholtz compositional energy and absorption change of $BZA_2PbBr_2I_2$ and $PEA_2PbBr_2I_2$ mixed halide perovskite

(A) Helmholtz compositional energy of $BZA_2PbBr_2I_2$ and $PEA_2PbBr_2I_2$. Dotted vertical lines serve to guide the eye.

(B and C) Changes in the absorption at peak wavelengths corresponding to Br, Br/I, and I peaks vs. illumination time at 25°C for (B) $BZA_2PbBr_2I_2$ and (C) $PEA_2PbBr_2I_2$.

Thus, we have selected BZA and PEA as model materials for a more detailed investigation, since the two spacers have very similar structure, differing only in the length of the alkyl chain on the phenyl ring (one and two carbon atoms for BZA and PEA, respectively). The X-ray diffraction (XRD) patterns of BZA-based and PEA-based perovskites are shown in Figure S1 and SEM cross-section of the films is shown in Figure S2, showing that in both cases thin films with similar thickness are obtained. To first examine the thermodynamic stability of these mixed perovskites, we calculated Helmholtz compositional energy[23] ΔF^0 for $PEA_2PbBr_2I_2$ and $BZA_2PbBr_2I_2$, as shown in Figure 2A. Helmholtz compositional energy as a function of temperature T is defined as:[23] $\Delta F^0(T) = \Delta U - T\Delta S(T)$, where ΔU is the mixing enthalpy and ΔS is the mixing entropy (calculations are described in more detail in STAR Methods). We can observe that $BZA_2PbBr_2I_2$ is unstable ($\Delta F^0 > 0$) for temperatures up to ~150°C, while $PEA_2PbBr_2I_2$ is stabilized by entropic effects already at low temperatures and is extremely stable at around room temperature. We have then examined PHS at low illumination power (6.5 mW/cm^2) where Helmholtz compositional energy dominates over photocarrier free energy. We can indeed observe significant segregation for BZA and suppressed segregation for PEA over entire temperature range, as shown in Figures S3 and S4. From the experimental data on the change of absorption for Br-rich, I/Br mixed region, and I-rich region, as shown in Figures 2B and 2C, we can observe a significant difference in the behavior of Br-rich region for BZA and PEA, since no Br-rich region forms for PEA. This difference between BZA and PEA persists at different temperatures, as shown in Figure S5 illustrating the change in the absorption at 85°C.

As the film preparation for each spacer cation has been optimized to achieve well-mixed starting film and consequently optimal annealing temperature differ, we have also performed PHS experiments for $BZA_2PbBr_2I_2$ films annealed at different temperatures, since films without secondary phases could be obtained over a wider range of temperatures compared to PEA. From Figure S6, we can observe that segregation occurs for all annealing temperatures, indicating that the observed differences can be attributed to the spacer cation used and not film annealing temperature. In addition, photoluminescence (PL) measurements were performed to confirm observed behavior differences between $BZA_2PbBr_2I_2$ and $PEA_2PbBr_2I_2$. As shown in Figure S7, significantly larger red shift is obtained for BZA-based perovskite compared to PEA-based perovskite. However, it should be noted that PL measurements have a drawback in characterizing PHS phenomenon, as the emission typically occurs from the lowest bandgap I-rich phase,[9,34,40] which was reported to account only for 1–2% of the mixed halide perovskite film.[34] In contrast, XRD and absorption spectroscopy probe all compositions in the film,[34] which makes absorption spectroscopy more suitable for comprehensive investigations of PHS.

Reversibility of PHS was investigated by maintaining the previously illuminated samples in the dark for a set period of time and performing absorption measurements. To examine the possible effects of the loss of volatile degradation products, both samples illuminated in inert environment without encapsulation are examined. Obtained results are shown in Figures S8 and S9. We can observe that encapsulation is necessary to ensure the reversibility of the process, in agreement with a previous report.[11] However, remixing process at room temperature for both $BZA_2PbBr_2I_2$ and $PEA_2PbBr_2I_2$ is very slow, with segregation persisting up to 48 h, different from a previous report on $BA_2PbBr_2I_2$ which exhibited complete remixing[9,11] on the timescale around one order of magnitude longer compared to time needed for PHS.[9] Possible reasons for the observed difference could be the use of different illumination source and different film microstructure (as the initial films exhibited very weak photoluminescence, as well as very fast PHS), as well as different spacer cation used. For $PEA_2PbBr_2I_2$, dark recovery was found to be incomplete[16] or absent,[20] which was attributed to nonbinomial halide distribution in $PEA_2PbBr_2I_2$, which results in additional energy barrier for Br^-/I^- to move into I/Br-rich octahedra.[20] Thus, very long time needed for remixing observed is in agreement with previous studies using the same spacer (PEA),[16,20] and likely due to the preferential halide distribution in axial and equatorial positions (see STAR Methods). When the samples are encapsulated and heated dark remixing occurs, as shown in Figure S9B and S9D, in agreement with observation of remixing at elevated temperature only for quasi-2D perovskite with PEA spacer cation.[20]

To explain significant differences in the emergence of Br-rich region in BZA and PEA, let us consider how PHS occurs. Halide segregation in both 3D and 2D perovskites involves iodide

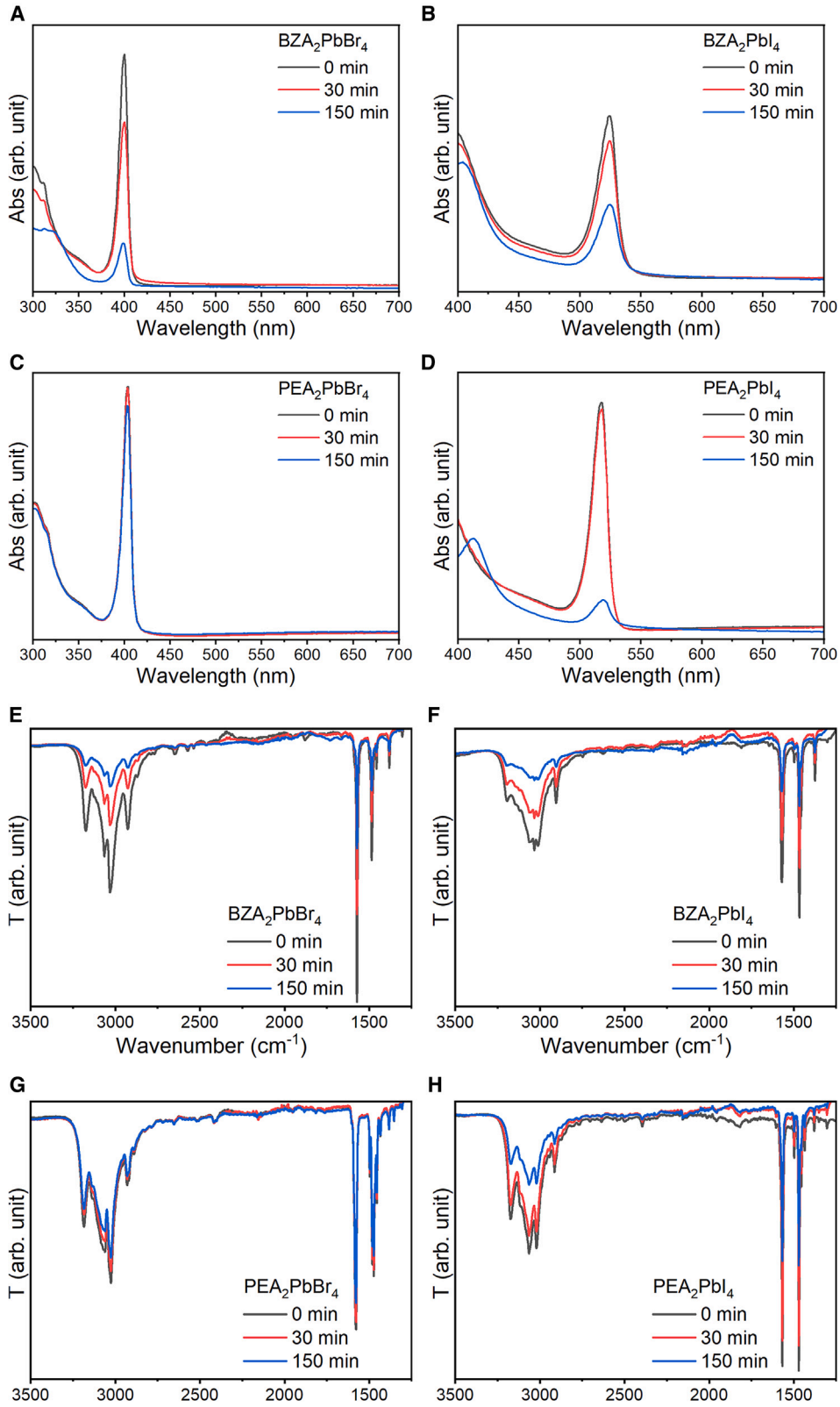

(legend on next page)

oxidation by photogenerated holes as an initial step, with subsequent formation of interstitial iodine and iodide vacancies, followed by halide migration, which then results in halide segregation and/or loss of iodide.[25,39,41] The photo/electrochemical nature of the reactions involved in PHS was confirmed by iodide expulsion experiments into the solution under illumination and/or bias, with the detection of oxidized iodide species (I_2 and I_3^-) in the solvent.[9,40] In addition, the critical role of organic cations in the degradation of 3D perovskites initiated by photogenerated or injected holes through photo/electrochemical processes has been elucidated recently.[39,42,43] It was found that perovskite decomposition occurs when both organic cations and lattice halides participate in electrochemical redox reactions,[42] and that organic ammonium cations are readily deprotonated by I_3^-,[43] which is a product of iodide oxidation. These processes include, but are not limited to, the following processes involving iodide (as there can be secondary reactions between different reaction products):[39–43] $I^- + h^+ \rightarrow I_i^0 + V_I$, $I_i^0 + h \rightarrow I_i^+$, $I_2 + I^- \leftrightarrow I_3^-$, $I_i^+ + I_i^+ \leftrightarrow I_2$, $I^- + 2h^+ \rightarrow I_i^+ + V_I^+$, $I_i^0 + e^- \rightarrow I_i^-$, $I_i^- + V_I^+ \rightarrow I^-$, $I_i^+ + V_I^+ + 2e^- \rightarrow I^-$, as well as reactions between oxidized halide and organic cation, such as $I_3^- + MA^+ \rightarrow MA + HI_3$, where I_i denotes iodine interstitial and V_I denotes iodine vacancy, MA^+ denotes CH_3NH_3 cation and MA denotes corresponding amine CH_3NH_2.

In contrast with 3D Perovskites, the PHS and ion migration are not as well understood in 2D perovskites. While it is known that the degradation of BA_2PbBr_4 under illumination involves the loss of BA cations,[44] and similar observation is made for BA_2PbI_4 and PEA_2PbI_4,[45] the role of cation loss in the photoinduced halide segregation and/or ion migration in 2D perovskites has not been investigated. As both PHS and instability of both mixed and pure halides under illumination are related to the trapping of holes on the halide, followed by the halide expulsion,[9] we investigated the photostability of pure bromide and iodide 2D perovskites. The stability tests were performed in dry air to accelerate the degradation due to the fact that oxygen serves as an electron scavenger, resulting in an excess of photogenerated holes[40] which then result in oxidation of iodide, triggering the chain reactions of perovskite decomposition.[25] From the absorption spectra of the 2D perovskite films illuminated in dry air shown in Figure 3, we can observe significant degradation for both BZA_2PbBr_4 and BZA_2PbI_4. Corresponding Fourier transform infrared spectroscopy (FTIR) spectra indicate clear loss of the organic cation, based on the weakening of various peaks corresponding to CH_x and NH_3 vibrations.[44] In contrast, while degradation is observed for PEA_2PbI_4 under illumination, in agreement with the literature,[5] PEA_2PbBr_4 exhibits good photostability and there is no weakening of organic cation vibration peaks in the corresponding FTIR spectra. This finding is in agreement with the lack of emergence of Br-rich region for $PEA_2PbBr_2I_2$ observed in our investigation, as well as previous report that PEA_2PbBr_4/PEA_2PbI_4 lateral heterostructures remained stable under UV illumination, while in quasi-2D $n = 2$ and $n = 3$ heterostructures loss of I occurred, followed by migration of Br into I-rich region.[21]

For other spacer cations investigated, we can observe a similar pattern, namely illumination in dry air leads to degradation of both endpoint halides (Figures S10–S13) for those spacers which exhibit significant PHS for mixed halide $A_2PbBr_2I_2$ perovskite (as shown in Figure 1). From absorption spectra and XRD patterns, we can observe that bromides are generally more photostable than iodides, and that stable bromide perovskite effectively suppresses segregation. In the case of bromides, we observe that PEA-, 4FPEA-, and TEA-based materials exhibit only a very small decrease on XRD intensity, without appearance of any new phases while the decrease in intensity is quite pronounced in the case of BA-, BZA-, HA-, and i-BA-based bromide perovskites. Different from bromides, in the case of iodides we observe significant decrease in the absorption peaks after illumination in almost all spacer cations (except for TEA). In addition to a decrease in intensities, low intensity peaks belonging to PbI_2 appear in XRD patterns of iodides (as well as other phases in the case of PEA, i-BA, and TMA). The observed lack of photostability in BA_2PbBr_4, and BA_2PbI_4 is in agreement with previous work, which showed that $BA_2PbI_2Br_2$, BA_2PbBr_4, and BA_2PbI_4 are unstable under illumination and bias, with expulsion of both I^- and Br^- detected.[9]

PHS in both 3D and 2D perovskites has been commonly explained considering the oxidation of halides by photogenerated holes, predominantly iodide as it has lower oxidation potential,[25,42,46] as well as lower bandgap resulting in hole accumulation in iodide-rich phase.[25] While both Br and I can be transported through the lattice by vacancy hopping, the preferential oxidation of lattice iodide resulting in iodine interstitials creates an imbalance in iodide and bromide transport.[46] However, photoelectrochemical reactions involve both oxidation and reduction reactions, and the involvement of organic cations in these reactions is evident from the cation movement across 3D/2D interfaces under illumination.[25,26] Thus, we propose that PHS in 2D perovskites involves both oxidation of halide by photogenerated holes, and reduction/deprotonation of organic cation by photogenerated electrons or oxidized halide species. Oxidized halide species, such as iodine interstitials (I_i, I_i^-, and I_i^+), molecular iodine (I_2), and triiodide (I_3^-), participate in various secondary reactions, which have been shown to include deprotonation of organic ammonium cations in 3D perovskites.[43] Deprotonation of organic cation would lead to the formation of cation vacancy, and spacer cation vacancies would lower the barrier for halide ion transport since spacer cations are responsible for suppression of ion migration in 2D perovskites.[3,5] If the spacer cations can react with oxidized halide species for both iodides and bromides, then a large number of spacer cation vacancies could readily form. On the other hand, the lack of reaction between spacer cation and oxidized bromide species, implied from photostability of A_2PbBr_4 perovskite, would lead to fewer vacancies of the spacer cations, which in turn inhibits the halide transport across the layers. The schematic diagram of the process for two types of 2D perovskites (with unstable and stable A_2PbBr_4 phases) is illustrated in Figure 4A.

Figure 3. Absorption and FTIR spectra of 2D Br-based or I-based perovskite under illumination

Absorption spectra of perovskite films illuminated under simulated solar illumination (100 mW/cm^2) for different times in dry air environment for (A) BZA_2PbBr_4, (B) BZA_2PbI_4, (C) PEA_2PbBr_4, and (D) PEA_2PbI_4; corresponding FTIR spectra of for (E) BZA_2PbBr_4, (F) BZA_2PbI_4, (G) PEA_2PbBr_4, and (H) PEA_2PbI_4.

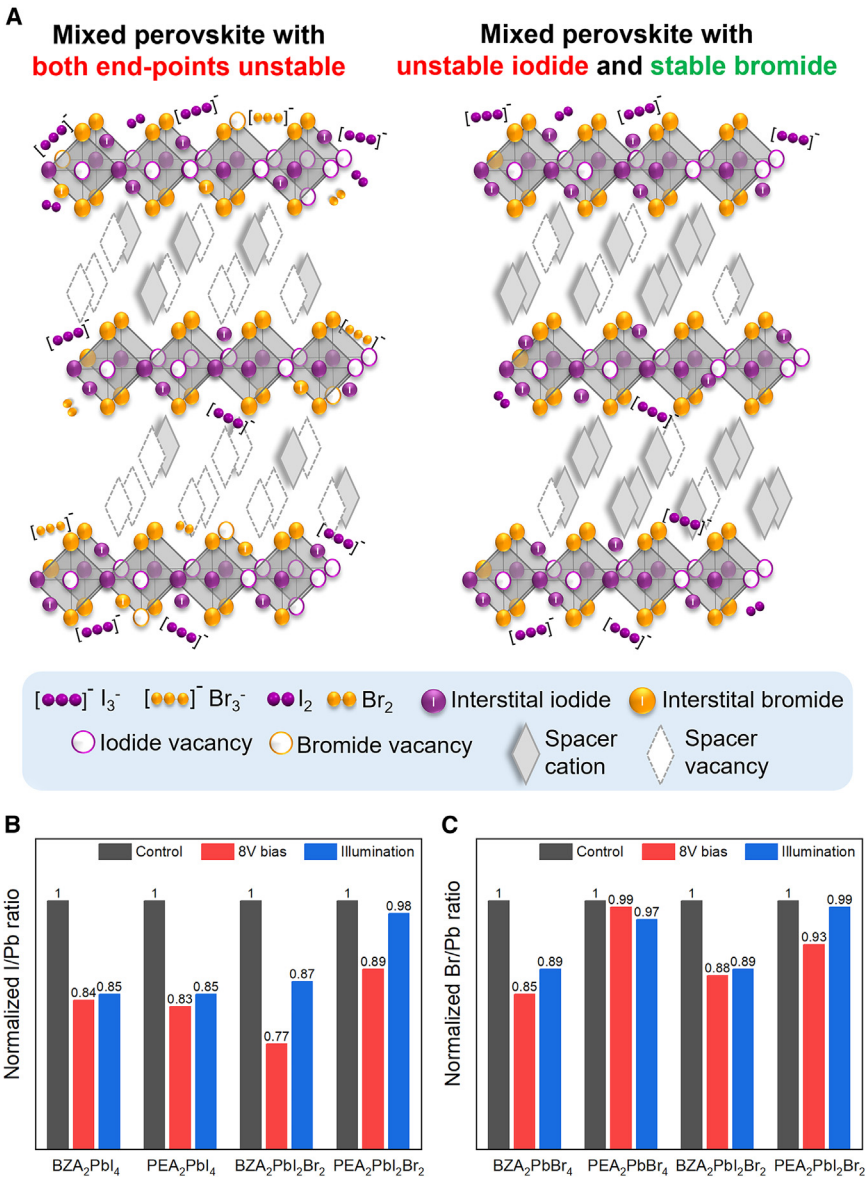

Figure 4. Schematic diagram and EDX measurent results

(A) Schematic diagram of photoelectrochemical reactions in the perovskites with both bromide and iodide phases susceptible to photooxidation (left) and only iodide phase susceptible to photooxidation (right); normalized halide:Pb ratios obtained from EDX measurements for different 2D perovskite films subjected to bias and illumination. The values have been normalized by halide content in the starting samples since we consider both A_2PbI_4 and $A_2PbI_2Br_2$.

(B) I:Pb.

(C) Br:Pb.

The proposed lack of interaction between oxidized bromide species and organic cation in photostable perovskites is also consistent with the fact that only iodide expulsion is observed from $MAPbBr_xI_{1-x}$, where MA denotes methylammonium,[40] where $MAPbBr_3$ has good photostability.[47,48] Due to differences in crystal structure (the lack of spacer cation barriers to ion transport[1,2,5] present in layered structures and the lack of different preferential occupation of axial and equatorial sites for Br^- and I^- which occurs in 2D perovskites[7,8]), PHS still occurs despite stable bromide perovskite for 3D materials. In contrast, for BA 2D perovskites both I^- and Br^- expulsion was detected, although slower rate was observed for Br^-,[9] in agreement with the proposed mechanism and the instability under illumination for both BA_2PbI_4 and BA_2PbBr_4 (Figures S10–S13). The involvement of an organic cation in the photo/electrochemical reactions leading to PHS and ion migration is also confirmed by the fact that no iodide expulsion in the solution is observed for Cs-based 3D perovskite,[49] where Cs^+ could be reduced by photogenerated electrons but cannot be deprotonated by oxidized iodide species. From the proposed mechanism, it follows that more significant segregation would be observed for higher iodine content for PEA_2PbBrI_3, as can indeed be observed in Figure S14, different from thermodynamically predicted higher stability for higher iodine content.[23] In all cases, $BZA_2PbBr_xI_{1-x}$ shows significant segregation, also shown in Figure S14. Finally, to further test the hypothesis of photo/electrochemical reactions, we prepared devices containing BZA- and PEA-based perovskite (pure Br, pure I, and Br:I 1:1) and subjected them to electrical bias or illumination without encapsulation and compared X:Pb (X = I, Br) ratio in fresh and aged perovskite films after removal of electrode and electron transport layer. Starting stoichiometry of the samples obtained from energy dispersive X-ray spectroscopy (EDX) measurements is shown in Table S2. Obtained results, shown in Figures 4B and 4C, clearly show same trends across different materials, although amount of halide loss for the same material varies on the stress type (bias, illumination). In BZA-based materials, both loss of iodide and bromide are detected for all compositions. For PEA-based samples under illumination, we observe significant loss of iodide for pure PEA_2PbI_4 only, while the loss of both bromide and iodide is negligible for $PEA_2PbBr_2I_2$, and the loss of bromide is negligible for pure PEA_2PbBr_4.

We have also examined the expulsion of halide into the toluene solution under illumination, as shown in Figure 5. Both films exhibit good stability in toluene without illumination for 1 h. For $BZA_2PbBr_2I_2$, we observe similar behavior as previously reported for $BA_2PbBr_2I_2$ in dichloromethane, namely disappearance of the mixed halide and I-rich phase peaks, with pure bromide phase peak persisting for some time after disappearance of

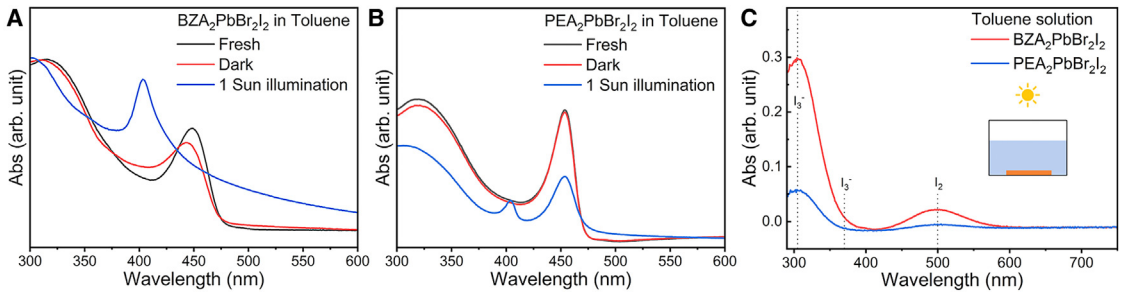

Figure 5. Absorption spectra of perovskite films and toluene solutions

(A and B) Absorption spectra of (A) $BZA_2PbBr_2I_2$ and (B) $PEA_2PbBr_2I_2$ films before and after immersion in toluene for 1 h in the dark and under illumination. (C) Absorption spectrum of toluene solution after the immersion of 2D perovskite films under 1 Sun illumination for 1 h.

mixed and I-rich phase.[9] In the case of $PEA_2PbBr_2I_2$, we can observe some loss of iodide phase, with illuminated films exhibiting clear mixed phase peak, as well as a smaller pure bromide peak, which can be attributed to the loss of iodide. From the absorption spectra of the toluene solutions after perovskite film immersion and illumination, Figure 5C, we can observe that expulsion of iodide is much smaller in the case of PEA-based perovskite, consisted with the changes in the absorption of films and overall observed behavior of PEA-based perovskite under illumination and bias.

From the obtained results, we can conclude that perovskites alkyl chain spacer cations generally have lower photostability. The presence of a ring (phenyl or thiophene) is not sufficient ensure photostability. There is a trend with respect to the length of alkyl chain attached to the ring, with spacer cations containing two carbon atoms chain (PEA, FPEA, and TEA) exhibiting good photostability, while those with one carbon atom (BZA and TMA) are susceptible to PHS and photoinduced degradation. As the spacer cations with three carbon atoms chain are also susceptible to PHS,[19] and the length of the alkyl chain affects the packing of the spacer cations and consequently their interactions, it is possible that ethyl chain attached to a phenyl or thiophene ring could lead to favorable conformal arrangements which would result in enhanced photostability. Alternatively, the length of the alkyl chain could affect the likelihood of deprotonation of the terminal ammonium group, which would also affect the photostability. In the absence of more comprehensive theoretical investigations looking into the effect of spacer cation structure and ordering on the 2D perovskite photostability, the photostability of pure bromide perovskite represents a good experimental predictor of the susceptibility of mixed halide perovskite to PHS and vice versa.

Conclusions

Thus, we show that PHS is suppressed in $A_2PbBr_2I_2$ 2D perovskites which exhibit photostable A_2PbBr_4 phase. From the known ability of triiodide I_3^- to deprotonate organic ammonium cations,[32] leading to desorption of organic amine and creation of organic cation vacancy, and the finding that most of the 2D iodide perovskites degrade under illumination, we propose that the lack of reaction between the spacer cation and oxidized bromide species is responsible for the suppression of PHS in $A_2PbBr_2I_2$ 2D perovskites with photostable A_2PbBr_4 phase. This results in fewer spacer cation vacancies compared to 2D perovskites where organic cation can react with both oxidized bromide and iodide species, leading to the desorption of amine and facilitation of interlayer ion transport.

Limitations of the study

We have considered eight different organic ammonium spacer cations which form 2D Ruddlesden-Popper organic lead halide perovskites to investigate their photoinduced halide segregation and photostability. While this is more comprehensive compared to other investigations in the literature and selected cations have different structures to ensure that general conclusions could be reached, there is a huge number of possible organic ammonium cations so that an exhaustive investigation of all possibilities is not practically feasible. Nevertheless, we believe that selected cations are sufficiently representative to ensure valid conclusions for the photostability of 2D Ruddlesden-Popper halide perovskites. However, the conclusions apply for the case where 2D perovskite is formed across all compositions; the discussion of ion migration barriers would not necessarily apply to any non-perovskite structures formed (for some spacer cations, it is possible that perovskite structures would form only for certain values of x in $A_2PbBr_xI_{1-x}$, for example for *tert*-butylammonium).

RESOURCE AVAILABILITY

Lead contact

Further information and requests for resources and materials should be directed to and will be fulfilled by the lead contact, Aleksandra B. Djurišić (dalek@hku.hk).

Materials availability

All materials used are commercially available and are used as received. This study did not generate new unique reagents.

Data and code availability

All data reported in this paper will be shared by the lead contact upon request. This paper does not report original code.

ACKNOWLEDGMENTS

This work was supported by the Seed Funding for Basic Research, the Seed Funding for Strategic Interdisciplinary Research Scheme, and Research Output Prize of the University of Hong Kong, RGC CRF project 7018-20G and NSFC project 6207032617. A.W.H.-B. is supported by the Australian

Research Council (ARC) Future Fellowship FT210100210. T. L. L. acknowledges support from the University of Sydney Faculty of Science Postgraduate Research Excellence Award (PREA).

AUTHOR CONTRIBUTIONS

Conceptualization, A.B.D., J.P., and T.L.L.; experimental measurements and figure plotting, Z.R., Z.Y., T.L.L., and Y.H.; calculations, J.O. and I.L.; supervision, A.B.D., A.W.Y.H.-B., and I.L.; writing the first draft, A.B.D.; writing-review and editing, A.B.D., J.P., .I.L, and A.W.Y.H.-B.

DECLARATION OF INTERESTS

The authors declare no conflict of interest.

STAR★METHODS

Detailed methods are provided in the online version of this paper and include the following:

- KEY RESOURCES TABLE
- METHOD DETAILS
  - Free energy calculations
  - Computational methods
  - Preparation of perovskite thin films
  - Thin film characterizations

SUPPLEMENTAL INFORMATION

Supplemental information can be found online at https://doi.org/10.1016/j.isci.2025.112154.

Received: November 7, 2024
Revised: December 24, 2024
Accepted: February 27, 2025
Published: March 4, 2025

REFERENCES

1. Gao, L., You, J., and Liu, S.F. (2021). Superior Photovoltaics/Optoelectronics of Two-Dimensional Halide Perovskites. J. Energy Chem. *57*, 69–82. https://doi.org/10.1016/j.jechem.2020.08.022.
2. Chen, J., Lee, D., and Park, N.-G. (2017). Stabilizing the Ag Electrode and Reducing J–V Hysteresis through Suppression of Iodide Migration in Perovskite Solar Cells. ACS Appl. Mater. Interfaces *9*, 36338–36349. https://doi.org/10.1021/acsami.7b07595.
3. Akriti, A., Shi, E., Shiring, S.B., Yang, J., Atencio-Martinez, C.L., Yuan, B., Hu, X., Gao, Y., Finkenauer, B.P., Pistone, A.J., et al. (2021). Layer-by-Layer Anionic Diffusion in Two-Dimensional Halide Perovskite Vertical Heterostructures. Nat. Nanotechnol. *16*, 584–591. https://doi.org/10.1038/s41565-021-00848-w.
4. Huang, W., Bu, T., Huang, F., and Cheng, Y.-B. (2020). Stabilizing High Efficiency Perovskite Solar Cells with 3D-2D Heterostructures. Joule *4*, 975–979. https://doi.org/10.1016/j.joule.2020.04.009.
5. Metcalf, I., Sidhik, S., Zhang, H., Agrawal, A., Persaud, J., Hou, J., Even, J., and Mohite, A.D. (2023). Synergy of 3D and 2D Perovskites for Durable, Efficient Solar Cells and Beyond. Chem. Rev. *123*, 9565–9652. https://doi.org/10.1021/acs.chemrev.3c00214.
6. Zhou, J., Wen, T., Sun, J., Shi, Z., Zou, C., Shen, Z., Li, Y., Wang, Y., Lin, Y., Yang, S., et al. (2024). Phase-Stable Wide-Bandgap Perovskites with 2D/3D Structure for All-Perovskite Tandem Solar Cells. ACS Energy Lett. *9*, 1984–1992. https://doi.org/10.1021/acsenergylett.4c00285.
7. Hope, M.A., Cordova, M., Mishra, A., Gunes, U., Caiazzo, A., Datta, K., Janssen, R.A.J., and Emsley, L. (2024). Axial–Equatorial Halide Ordering in Layered Hybrid Perovskites from Isotropic–Anisotropic ^{207}Pb NMR. Angew. Chem. Int. Ed. *63*, e202314856. https://doi.org/10.1002/anie.202314856.
8. Toso, S., Gushchina, I., Oliver, A.G., Manna, L., and Kuno, M. (2022). Are Mixed-Halide Ruddlesden–Popper Perovskites Really Mixed? ACS Energy Lett. *7*, 4242–4247. https://doi.org/10.1021/acsenergylett.2c01967.
9. Mathew, P.S., Szabó, G., Kuno, M., and Kamat, P.V. (2022). Phase Segregation and Sequential Expulsion of Iodide and Bromide in Photoirradiated Ruddlesden–Popper 2D Perovskite Films. ACS Energy Lett. *7*, 3982–3988. https://doi.org/10.1021/acsenergylett.2c02026.
10. Liu, Y., Wang, M., Ievlev, A.V., Ahmadi, A., Keum, J.K., Ahmadi, M., Hu, B., and Ovchinnikova, O.S. (2022). Photoinduced Iodide Repulsion and Halides-Demixing in Layered Perovskites. Mater. Today Nano *18*, 100197. https://doi.org/10.1016/j.mtnano.2022.100197.
11. Mathew, P.S., DuBose, J.T., Cho, J., and Kamat, P.V. (2021). Spacer Cations Dictate Photoinduced Phase Segregation in 2D Mixed Halide Perovskites. ACS Energy Lett. *6*, 2499–2501. https://doi.org/10.1021/acsenergylett.1c01015.
12. Akriti, A., Zhang, S., Lin, Z.-Y., Shi, E., Finkenauer, B.P., Gao, Y., Pistone, A.J., Ma, K., Savoie, B.M., and Dou, L. (2021). Quantifying Anionic Diffusion in 2D Halide Perovskite Lateral Heterostructures. Adv. Mater. *33*, 2105183. https://doi.org/10.1002/adma.202105183.
13. Wang, Y.-R., Senocrate, A., Mladenović, M., Dučinskas, A., Kim, G.Y., Rothlisberger, U., Milić, J.V., Moia, D., Grätzel, M., and Maier, J. (2022). Photo De-Mixing in Dion-Jacobson 2D Mixed Halide Perovskites. Adv. Energy Mater. *12*, 2200768. https://doi.org/10.1002/aenm.202200768.
14. Yadav, A.N., Min, S., Choe, H., Park, J., and Cho, J. (2024). Halide Ion Mixing across Colloidal 2D Ruddlesden-Popper Perovskites: Implication of Spacer Ligand on Mixing Kinetics. Small *20*, 2305546. https://doi.org/10.1002/smll.202305546.
15. Akriti, A., Lin, Z.-Y., Park, J.Y., Yang, H., Savoie, B.M., and Dou, L. (2022). Anion Diffusion In Two-Dimensional Halide Perovskites. APL Mater. *10*, 040903. https://doi.org/10.1063/5.0088538.
16. Cho, J., Mathew, P.S., DuBose, J.T., and Kamat, P.V. (2021). Photoinduced Halide Segregation in Ruddlesden–Popper 2D Mixed Halide Perovskite Films. Adv. Mater. *33*, 2105585. https://doi.org/10.1002/adma.202105585.
17. Cho, J., DuBose, J.T., Le, A.N.T., and Kamat, P.V. (2020). Suppressed Halide Ion Migration in 2D Lead Halide Perovskites. ACS Mater. Lett. *2*, 565–570. https://doi.org/10.1021/acsmaterialslett.0c00124.
18. Min, S., and Cho, J. (2024). Halide Ion Mobility in Paired 2D Halide Perovskites: Ruddlesden–Popper Versus Dion–Jacobson Phases. Adv. Opt. Mater. *12*, 2302516. https://doi.org/10.1002/adom.202302516.
19. Leung, T.L., Ren, Z., Syed, A.A., Grisanti, L., Djurišić, A.B., and Popović, J. (2022). Photoinduced Segregation Behavior in 2D Mixed Halide Perovskite: Effects of Light and Heat. ACS Energy Lett. *7*, 3500–3508. https://doi.org/10.1021/acsenergylett.2c01688.
20. Datta, K., Caiazzo, A., Hope, M.A., Li, J., Mishra, A., Cordova, M., Chen, Z., Emsley, L., Wienk, M.M., and Janssen, R.A.J. (2023). Light-Induced Halide Segregation in 2D and Quasi-2D Mixed-Halide Perovskites. ACS Energy Lett. *8*, 1662–1670. https://doi.org/10.1021/acsenergylett.3c00160.
21. Luo, Y., Zhang, S., Chen, J.-S., Ma, X., Ma, K., Deng, J., Jiang, Y., Li, L., Lai, B., Chen, S., et al. (2023). Photo-Induced Halide Redistribution in 2D Halide Perovskite Lateral Heterostructures. Joule *7*, 2376–2385. https://doi.org/10.1016/j.joule.2023.08.003.
22. Wei, G., Kaplan, A.B., Zhang, H., Loo, Y.-L., and Webb, M.A. (2024). Effects of Ligand Chemistry on Ion Transport in 2D Hybrid Organic–Inorganic Perovskites. Adv. Energy Mater. *14*, 2401087. https://doi.org/10.1002/aenm.202401087.
23. Chen, Z., Xue, H., Brocks, G., Bobbert, P.A., and Tao, S. (2023). Thermodynamic Origin of the Photostability of the Two-Dimensional Perovskite $PEA_2Pb(I_{1-x}Br_x)_4$. ACS Energy Lett. *8*, 943–949. https://doi.org/10.1021/acsenergylett.2c02463.

24. Mathew, P.S., and Kamat, P.V. (2024). Cation Migration in Physically Paired 2D and 3D Lead Halide Perovskite Films. Adv. Opt. Mater. *12*, 2300957. https://doi.org/10.1002/adom.202300957.

25. Mathew, P., Cho, J., and Kamat, P.V. (2024). Ramifications of Ion Migration in 2D Lead Halide Perovskites. ACS Energy Lett. *9*, 1103–1114. https://doi.org/10.1021/acsenergylett.4c00093.

26. Chakkamalayath, J., Hiott, N., and Kamat, P.V. (2023). How Stable is the 2D/3D Interface of Metal Halide Perovskite under Light and Heat? ACS Energy Lett. *8*, 169–171. https://doi.org/10.1021/acsenergylett.2c02408.

27. Moral, R.F., Perini, C.A.R., Kodalle, T., Kim, A., Babbe, F., Harada, N., Hajhemati, J., Schulz, P., Ginsberg, N.S., Aloni, S., et al. (2024). Anion and Cation Migration at 2D/3D Halide Perovskite Interfaces. ACS Energy Lett. *9*, 2703–2716. https://doi.org/10.1021/acsenergylett.4c00728.

28. Knight, A.J., Patel, J.B., Snaith, H.J., Johnston, M.B., and Herz, L.M. (2020). Trap States, Electric Fields, and Phase Segregation in Mixed-Halide Perovskite Photovoltaic Devices. Adv. Energy Mater. *10*, 1903488. https://doi.org/10.1002/aenm.201903488.

29. Barker, A.J., Sadhanala, A., Deschler, F., Gandini, M., Senanayak, S.P., Pearce, P.M., Mosconi, E., Pearson, A.J., Wu, Y., Srimath Kandada, A.R., et al. (2017). Defect-Assisted Photoinduced Halide Segregation in Mixed-Halide Perovskite Thin Films. ACS Energy Lett. *2*, 1416–1424. https://doi.org/10.1021/acsenergylett.7b00282.

30. Zhou, Y., van Laar, S.C.W., Meggiolaro, D., Gregori, L., Martani, S., Heng, J.Y., Datta, K., Jiménez-López, J., Wang, F., Wong, E.L., et al. (2024). How Photogenerated I_2 Induces I-Rich Phase Formation in Lead Mixed Halide Perovskites. Adv. Mater. *36*, 2305567. https://doi.org/10.1002/adma.202305567.

31. Zhou, Y., Wong, E.L., Folpini, G., Zanolini, M., Jiménez-López, J., Treglia, A., and Petrozza, A. (2024). Mutual Destabilization of Wide Bandgap Perovskite and PbI_2 Inclusions through Interface Carrier Trapping. Adv. Funct. Mater. *34*, 2406317. https://doi.org/10.1002/adfm.202406317.

32. Chen, Z., Brocks, G., Tao, S., and Bobbert, P.A. (2021). Unified Theory for Light-Induced Halide Segregation in Mixed Halide Perovskites. Nat. Commun. *12*, 2687. https://doi.org/10.1038/s41467-021-23008-z.

33. Okrepka, H., Ding, Y., Ghonge, S., Ruth, A., and Kuno, M. (2024). Excitation Intensity-Dependent Terminal Halide Photosegregation Stoichiometries in Formamidinium/Cesium Lead Iodide/Bromide [$FACsPb(I_{1-x}Br_x)_3$] Thin Films. J. Phys. Chem. Lett. *15*, 10488–10494. https://doi.org/10.1021/acs.jpclett.4c02008.

34. Ruth, A., and Kuno, M. (2023). Modeling the Photoelectrochemical Evolution of Lead-Based, Mixed-Halide Perovskites due to Photosegregation. ACS Nano *17*, 20502–20511. https://doi.org/10.1021/acsnano.3c07165.

35. Choe, H., Jeon, D., Lee, S.J., and Cho, J. (2021). Mixed or Segregated: Toward Efficient and Stable Mixed Halide Perovskite-Based Devices. ACS Omega *6*, 24304–24315. https://doi.org/10.1021/acsomega.1c03714.

36. Ruth, A., Okrepka, H., Kamat, P., and Kuno, M. (2023). Thermodynamic Band Gap Model for Photoinduced Phase Segregation in Mixed-Halide Perovskites. J. Phys. Chem. C *127*, 18547–18559. https://doi.org/10.1021/acs.jpcc.3c04708.

37. Limmer, D.T., and Ginsberg, N.S. (2020). Photoinduced Phase Separation in the Lead Halides is a Polaronic Effect. J. Chem. Phys. *152*, 230901. https://doi.org/10.1063/1.5144291.

38. Bischak, C.G., Wong, A.B., Lin, E., Limmer, D.T., Yang, P., and Ginsberg, N.S. (2018). Tunable Polaron Distortions Control the Extent of Halide Demixing in Lead Halide Perovskites. J. Phys. Chem. Lett. *9*, 3998–4005. https://doi.org/10.1021/acs.jpclett.8b01512.

39. Ali, M.U., Mo, H., Rehman, A.U., Leung, T.L., and Djurišić, A.B. (2024). Metal Halide Perovskites: Stability under Illumination and Bias. Trends Chem. *6*, 248–259. https://doi.org/10.1016/j.trechm.2024.03.009.

40. DuBose, J.T., and Kamat, P.V. (2022). Hole Trapping in Halide Perovskites Induces Phase Segregation. Acc. Mater. Res. *3*, 761–771. https://doi.org/10.1021/accountsmr.2c00076.

41. Xu, Z., Kerner, R.A., Kronik, L., and Rand, B.P. (2024). Beyond Ion Migration in Metal Halide Perovskites: Toward a Broader Photoelectrochemistry Perspective. ACS Energy Lett. *9*, 4645–4654. https://doi.org/10.1021/acsenergylett.4c02033.

42. Xu, Z., Kerner, R.A., Berry, J.J., and Rand, B.P. (2022). Iodine Electrochemistry Dictates Voltage-Induced Halide Segregation Thresholds in Mixed-Halide Perovskite Devices. Adv. Funct. Mater. *32*, 2203432. https://doi.org/10.1002/adfm.202203432.

43. Hu, J., Xu, Z., Murrey, T.L., Pelczer, I., Kahn, A., Schwartz, J., and Rand, B.P. (2023). Triiodide Attacks the Organic Cation in Hybrid Lead Halide Perovskites: Mechanism and Suppression. Adv. Mater. *35*, 2303373. https://doi.org/10.1002/adma.202303373.

44. Zhong, C., Che, X., Xu, C., Chen, C., Yang, C., and Zhu, Y. (2024). Instability of Two-Dimensional Hybrid Perovskites Underpinned by Organic Molecule Loss under Light Illumination. Mater. Chem. Front. *8*, 2836–2844. https://doi.org/10.1039/D4QM00324A.

45. Ren, Z., Ovčar, J., Leung, T.L., He, Y., Li, Y., Li, D., Qin, X., Mo, H., Yuan, Z., Bing, J., et al. (2025). Increased Resistance to Photooxidation in Dion-Jacobson Lead Halide Perovskites: Implication for Perovskite Device Stability. Matter *8*, 101937. https://doi.org/10.1016/j.matt.2024.11.031.

46. Xu, Z., Kerner, R.A., Harvey, S.P., Zhu, K., Berry, J.J., and Rand, B.P. (2023). Halogen Redox Shuttle Explains Voltage-Induced Halide Redistribution in Mixed-Halide Perovskite Devices. ACS Energy Lett. *8*, 513–520. https://doi.org/10.1021/acsenergylett.2c02385.

47. Pont, S., Bryant, D., Lin, C.-T., Aristidou, N., Wheeler, S., Ma, X., Godin, R., Haque, S.A., and Durrant, J.R. (2017). Tuning $CH_3NH_3Pb(I_{1-x}Br_x)_3$ Perovskite Oxygen Stability in Thin Films and Solar Cells. J. Mater. Chem. A *5*, 9553–9560. https://doi.org/10.1039/C7TA00058H.

48. Aziz, A., Aristidou, N., Bu, X., Westbrook, R.J.E., Haque, S.A., and Islam, M.S. (2020). Understanding the Enhanced Stability of Bromide Substitution in Lead Iodide Perovskites. Chem. Mater. *32*, 400–409. https://doi.org/10.1021/acs.chemmater.9b04000.

49. Mathew, P.S., Samu, G.F., Janáky, C., and Kamat, P.V. (2020). Iodine (I) Expulsion at Photoirradiated Mixed Halide Perovskite Interface. Should I Stay or Should I Go? ACS Energy Lett. *5*, 1872–1880. https://doi.org/10.1021/acsenergylett.0c00925.

50. Wright, N.E., Qin, X., Xu, J., Kelly, L.L., Harvey, S.P., Toney, M.F., Blum, V., and Stiff-Roberts, A.D. (2022). Influence of Annealing and Composition on the Crystal Structure of Mixed-Halide, Ruddlesden–Popper Perovskites. Chem. Mater. *34*, 3109–3122. https://doi.org/10.1021/acs.chemmater.1c04213.

51. Ovčar, J., Leung, T.L., Grisanti, L., Skoko, Ž., Vrankić, M., Low, K.-H., Wang, S., You, P.-Y., Ahn, H., Lončarić, I., et al. (2022). Mixed Halide Ordering as a Tool for the Stabilization of Ruddlesden–Popper Structures. Chem. Mater. *34*, 4286–4297. https://doi.org/10.1021/acs.chemmater.1c03815.

52. Giannozzi, P., Baroni, S., Bonini, N., Calandra, M., Car, R., Cavazzoni, C., Ceresoli, D., Chiarotti, G.L., Cococcioni, M., Dabo, I., et al. (2009). QUANTUM ESPRESSO: a Modular and Open-Source Software Project for Quantum Simulations of Materials. J. Phys. Condens. Matter *21*, 395502. https://doi.org/10.1088/0953-8984/21/39/395502.

53. Giannozzi, P., Andreussi, O., Brumme, T., Bunau, O., Buongiorno Nardelli, M., Calandra, M., Car, R., Cavazzoni, C., Ceresoli, D., Cococcioni, M., et al. (2017). Advanced Capabilities for Materials Modelling with Quantum ESPRESSO. J. Phys. Condens. Matter *29*, 465901. https://doi.org/10.1088/1361-648X/aa8f79.

54. Thonhauser, T., Cooper, V.R., Li, S., Puzder, A., Hyldgaard, P., and Langreth, D.C. (2007). Van der Waals Density Functional: Self-Consistent Potential and the Nature of the Van Der Waals Bond. Phys. Rev. B *76*, 125112. https://doi.org/10.1103/PhysRevB.76.125112.

55. Langreth, D.C., Lundqvist, B.I., Chakarova-Käck, S.D., Cooper, V.R., Dion, M., Hyldgaard, P., Kelkkanen, A., Kleis, J., Kong, L., Li, S., et al. (2009). A Density Functional for Sparse Matter. J. Phys. Condens. Matter *21*, 084203. https://doi.org/10.1088/0953-8984/21/8/084203.

56. Thonhauser, T., Zuluaga, S., Arter, C.A., Berland, K., Schröder, E., and Hyldgaard, P. (2015). Spin Signature of Nonlocal Correlation Binding in Metal-Organic Frameworks. Phys. Rev. Lett. *115*, 136402. https://doi.org/10.1103/PhysRevLett.115.136402.

57. Berland, K., Cooper, V.R., Lee, K., Schröder, E., Thonhauser, T., Hyldgaard, P., and Lundqvist, B.I. (2015). Van der Waals Forces in Density Functional Theory: a Review of the vdW-DF Method. Rep. Prog. Phys. *78*, 066501. https://doi.org/10.1088/0034-4885/78/6/066501.

58. Garrity, K.F., Bennett, J.W., Rabe, K.M., and Vanderbilt, D. (2014). Pseudopotentials for High-Throughput DFT Calculations. Comput. Mater. Sci. *81*, 446–452. https://doi.org/10.1016/j.commatsci.2013.08.053.

59. Monkhorst, H.J., and Pack, J.D. (1976). Special Points for Brillouin-Zone Integrations. Phys. Rev. B *13*, 5188–5192. https://doi.org/10.1103/PhysRevB.13.5188.

60. Smith, M.D., Jaffe, A., Dohner, E.R., Lindenberg, A.M., and Karunadasa, H.I. (2017). Structural Origins of Broadband Emission from Layered Pb–Br Hybrid Perovskites. Chem. Sci. *8*, 4497–4504. https://doi.org/10.1039/C7SC01590A.

61. Du, K.-z., Tu, Q., Zhang, X., Han, Q., Liu, J., Zauscher, S., and Mitzi, D.B. (2017). Two-Dimensional Lead(II) Halide-Based Hybrid Perovskites Templated by Acene Alkylamines: Crystal Structures, Optical Properties, and Piezoelectricity. Inorg. Chem. *56*, 9291–9302. https://doi.org/10.1021/acs.inorgchem.7b01094.

62. Jiang, Y., and Yuan, M. (2020). CCDC 2006717: Experimental Crystal Structure Determination. https://doi.org/10.5517/ccdc.csd.cc25c4tj.

63. Jung, M.-H. (2019). Hydrophobic Perovskites Based on an Alkylamine Compound for High Efficiency Solar Cells with Improved Environmental Stability. J. Mater. Chem. A *7*, 14689–14704. https://doi.org/10.1039/C9TA01569H.

64. Dammak, H., Elleuch, S., Feki, H., and Abid, Y. (2016). Synthesis, Crystal Structure, Vibrational Spectra, Optical Properties and Theoretical Investigation of a Two-Dimensional Self-Assembled Organic-Inorganic Hybrid Material. Solid State Sci. *61*, 1–8. https://doi.org/10.1016/j.solidstatesciences.2016.08.014.

65. Zhu, X.-H., Mercier, N., Riou, A., Blanchard, P., and Frère, P. (2002). $(C_4H_3SCH_2NH_3)_2(CH_3NH_3)Pb_2I_7$: Non-Centrosymmetrical Crystal Structure of a Bilayer Hybrid Perovskite. Chem. Commun., 2160–2161. https://doi.org/10.1039/B205543K.

66. Sheikh, T., Shinde, A., Mahamuni, S., and Nag, A. (2018). Possible Dual Bandgap in $(C_4H_9NH_3)_2PbI_4$ 2D Layered Perovskite: Single-Crystal and Exfoliated Few-Layer. ACS Energy Lett. *3*, 2940–2946. https://doi.org/10.1021/acsenergylett.8b01799.

67. Kamminga, M.E., Fang, H.-H., Filip, M.R., Giustino, F., Baas, J., Blake, G.R., Loi, M.A., and Palstra, T.T.M. (2016). Confinement Effects in Low-Dimensional Lead Iodide Perovskite Hybrids. Chem. Mater. *28*, 4554–4562. https://doi.org/10.1021/acs.chemmater.6b00809.

68. Gao, P. (2018). CCDC 1878698: Experimental Crystal Structure Determination. https://doi.org/10.5517/ccdc.csd.cc211y57.

69. Hoffman, J.M., Malliakas, C.D., Sidhik, S., Hadar, I., McClain, R., Mohite, A.D., and Kanatzidis, M.G. (2020). Long Periodic Ripple in a 2D Hybrid Halide Perovskite Structure Using Branched Organic Spacers. Chem. Sci. *11*, 12139–12148. https://doi.org/10.1039/D0SC04144K.

70. Wang, Z.-X., Liao, W.-Q., Ye, H.-Y., and Zhang, Y. (2015). Sequential Structural Transitions with Distinct Dielectric Responses in a Layered Perovskite Organic–Inorganic Hybrid Material: $[C_4H_9N]_2[PbBr_4]$. Dalton Trans. *44*, 20406–20412. https://doi.org/10.1039/C5DT03277F.

STAR★METHODS

KEY RESOURCES TABLE

REAGENT or RESOURCE	SOURCE	IDENTIFIER
Chemicals, peptides, and recombinant proteins		
N,N-dimethylformamide (DMF, anhydrous, 99.9%)	Thermo Scientific Chemicals	CAS: 68-12-2
Dimethyl Sulfoxide (DMSO, anhydrous, ≥99.9%)	Sigma-Aldrich	CAS: 67-68-5
Lead(II) bromide ($PbBr_2$, ≥98%)	Tokyo Chemical Industry	CAS: 10031-22-8
Lead(II) iodide (PbI_2, ≥98%)	Tokyo Chemical Industry	CAS: 10101-63-0
(2-(9H-carbazol-9-yl)ethyl)phosphonic acid (2PACz, >98.0%)	Tokyo Chemical Industry	CAS: 20999-38-6
γ-butyrolactone (GBL, >99.0%)	Tokyo Chemical Industry	CAS: 96-48-0
n-butylammonium bromide (n-BABr)	Greatcell Solar	CAS: 15567-09-6
n-butylammonium iodide (n-BAI)	Greatcell Solar	CAS: 36945-08-1
iso-butylammonium bromide (i-BABr)	Greatcell Solar	CAS: 74098-36-5
iso-butylammonium iodide (i-BAI)	Greatcell Solar	CAS: 205508-75-4
n-hexylammonium bromide (HABr)	Greatcell Solar	CAS: 7334-95-4
n-hexylammonium iodide (HAI)	Greatcell Solar	CAS: 54285-91-5
benzylammonium bromide (BZABr)	Greatcell Solar	CAS: 37488-40-7
benzylammonium iodide (BZAI)	Greatcell Solar	CAS: 45579-91-7
phenethylammonium bromide (PEABr)	Greatcell Solar	CAS: 53916-94-2
phenethylammonium iodide (PEAI)	Greatcell Solar	CAS: 151059-43-7
4-fluoro-phenethylammonium bromide (4FPEABr)	Greatcell Solar	CAS: 1807536-06-6
4-fluoro-phenethylammonium iodide (4FPEAI)	Greatcell Solar	CAS: 1413269-55-2
2-thiopheneethylammonium bromide (TEABr)	Greatcell Solar	CAS: 2490324-60-0
2-thiopheneethylammonium iodide (TEAI)	Greatcell Solar	CAS: 2414055-94-8
2-thiophenemethylammonium iodide (TMAI)	Greatcell Solar	CAS: 2247100-32-7
2-thiophenemethyl ammonium bromide (TMABr)	Xi'an Yuri	CAS: 59852-33-4
(6,6)-Phenyl C61 butyric acid methyl ester (PCBM, >99.8%)	Luminescence Technology	CAS: 160848-22-6
bathocuproine (BCP, >99.5%)	Luminescence Technology	CAS: 4733-39-5
Isopropyl alcohol (IPA, 99.5%)	Anaqua	CAS: 67-63-0
ethanol (99.9%)	Anaqua	CAS: 64-17-5
Other		
Agilent Cary 60 UV-Vis spectrometer	Agilent	https://www.agilent.com/en/product/molecular-spectroscopy/uv-vis-uv-vis-nir-spectroscopy/uv-vis-uv-vis-nir-systems/cary-60-uv-vis-spectrophotometer
PDA-512 USB fiberoptic spectrometer	Control Development	http://www.controldevelopment.com/products/spectrometers/product-spectrometers-silicon-pda.php
Sunbrick™ Solar Simulator	G2V	https://g2voptics.com/products/led-solar-simulator-sunbrick/
Xenon lamp	Newport	https://www.newport.com/p/66906-150XF-R15
UV-curing Resin 3055B	ThreeBond	https://www.threebond.co.jp/en/product/threebond_3055b/
MiniFlex 600-C X-ray Diffractometer	Rigaku	https://rigaku.com/products/x-ray-diffraction-and-scattering/xrd/miniflex
Spectrum Two ATR-FTIR spectrometer	PerkinElmer	https://www.perkinelmer.com/Product/spectrum-two-ft-ir-sp10-software-l160000a

(*Continued on next page*)

Continued

REAGENT or RESOURCE	SOURCE	IDENTIFIER
S4800 FEG SEM	Hitachi	https://www.hitachi-hightech.com/global/en/products/microscopes/sem-tem-stem/fe-sem/
Keithley's Standard Series 2400 Source Measure Unit	Tektronix Technologies	https://www.tek.com/en/products/keithley/source-measure-units/2400-standard-series-sourcemeter
XploRA Plus Raman/PL spectrometer	Horiba	https://www.horiba.com/int/scientific/products/detail/action/show/Product/xploratm-plus-1528/
SU8230 FEG SEM	Hitachi	https://www.hitachi-hightech.com/global/en/products/microscopes/sem-tem-stem/fe-sem/
Ultim Max EDS detector	Oxford Instruments	https://nano.oxinst.com/products/ultim-max

METHOD DETAILS

Free energy calculations

Our aim is to estimate the free energy under illumination of mixed-halide Ruddlesden-Popper perovskites $PEA_2PbBr_2I_2$ and $BZA_2PbBr_2I_2$. The temperature-dependent free energy is:[23]

$$\Delta F(T) = \Delta F^0(T) + \Delta F^*(T) \quad \text{(Equation 1)}$$

where ΔF^0 is the Helmholtz compositional energy and ΔF^* is the photocarrier free energy. ΔF^0 is defined as:

$$\Delta F^0(T) = \Delta U - T\Delta S(T) \quad \text{(Equation 2)}$$

where ΔU is the mixing enthalpy and ΔS is the mixing entropy. ΔU is given by:

$$\Delta U = E_M - 0.5\,(E_{Br} + E_I) \quad \text{(Equation 3)}$$

where E_M, E_{Br} and E_I are the total energies per formula unit (f.u.) of the mixed I-Br and pure Br and I phases, respectively. Finally, for our use-case of identical bromide and iodine concentrations, the mixing entropy provides a constant contribution:

$$\Delta S = -3\,ln(2)k_B \quad \text{(Equation 4)}$$

where k_B is the Boltzmann constant. At a given temperature, if $\Delta F\,(T) > 0$, the halide-segregated phase is (meta)stable under illumination, while the mixed phase is (meta)stable if $\Delta F(T) < 0$. Similarly, $\Delta F^0(T) > 0$ indicates stability of the segregated phase and $\Delta F^0(T) < 0$ indicates stability of the mixed phase in the dark.

The crystal structure of $PEA_2PbBr_2I_2$ has been previously experimentally determined.[50] Similarly to $(t\text{-}BA)_2PbBr_2I_2$[51] and $BZA_2PbBr_2I_2$,[8] the halide distribution exhibits high structural ordering, with one species being almost exclusively found at equatorial positions of the perovskite layers, while the other is found at axial positions.

On the other hand, the crystal structure of $BZA_2PbBr_2I_2$ has not been experimentally determined. Our powder X-ray measurements show that the length of the c-axis of the unit cell amounts to 32.872(1) Å which is similar to the length of the c-axis of the pure bromide-based perovskite BZA_2PbBr_4 (33.35 Å). Therefore, we constructed guess- structures for $BZA_2PbBr_2I_2$ by substituting half of the bromide atoms in the experimentally determined structure of BZA_2PbBr_4 with iodines. As in our previous investigation,[51] we performed the substitution in three ways, resulting in three guess-structures with the following halide distributions:

(a) bromides in axial positions, iodines in equatorial positions;
(b) iodines in axial positions, bromides in equatorial positions;
(c) iodines and bromides alternately occupying halide lattice sites.

Starting from such guess structures, we optimized the atomic positions and unit cell parameters as described in the computational methods and compared the computed energies. We find that configuration (b) is the most stable, with configurations (a) and (c) being higher in energy by 0.12 eV/f.u. and 0.02 eV/f.u, respectively.

The halide distribution in the experimentally determined $PEA_2PbBr_2I_2$ crystal structure is the same as configuration (b) described above. We performed analogous computations on hypothetical $PEA_2PbBr_2I_2$ structures with halide configurations (a) and (c). We obtain that configuration (b) is indeed the most stable one, with configurations (a) and (c) being higher in energy by 0.14 eV/f.u. and 0.03 eV/f.u., closely resembling the trend observed for BZA_2PbI_4.

From the plot of the Helmholtz compositional energy ΔF^0 for $PEA_2PbBr_2I_2$ and $BZA_2PbBr_2I_2$, shown in Figure 2A, of the main manuscript. We can see that $BZA_2PbBr_2I_2$ is unstable over a large range of temperatures, while $PEA_2PbBr_2I_2$ is stabilized by entropic effects already at low temperatures and is extremely stable at around room temperature.

It is worthwhile to note that we are using a theoretically obtained structure for $BZA_2PbBr_2I_2$, $BZA_2PbBr_2I_2$ which increases uncertainty in the corresponding calculated Helmholtz compositional energy. However, given the very large difference in the calculated enthalpies between the two systems ($\approx$ 0.06 eV/f.u.), we may safely draw the main qualitative conclusion: the mixed-halide perovskite phase based on PEA is compositionally significantly more stable compared to the analogous phase based on BZA.

Under low illumination intensity, we expect that Helmholtz compositional energy will be the dominant factor contributing to free energy. To verify this, the photocarrier free energy ΔF*may be estimated as

$$\Delta F^* = nE_g \quad \text{(Equation 5)}$$

where n is the photocarrier density (number of photocarriers per f.u.) and E_g is the band gap of the mixed-halide phase.[23] We have calculated the band gaps of $BZA_2PbBr_2I_2$ and $PEA_2PbBr_2I_2$ and obtained the values 2.47 eV and 2.41 eV, respectively. The photocarrier density n may be approximated as:[23]

$$n = G\tau \quad \text{(Equation 6)}$$

where G is the photocarrier generation rate and τ is the photocarrier lifetime. G is given by:

$$G = I\alpha V/h\nu \quad \text{(Equation 7)}$$

where I is the illumination intensity, α is the absorption coefficient, V is the volume per f.u. and hν is the photon energy. Taking the same values as were taken in the literature for $PEA_2Pb(Br_xI_{1-x})_4$ ($\alpha = 10^{-5}$ cm^{-1}, $V = 2.5 \times 10^{-22}$ cm^3, hν = 3 eV), the appropriate photocarrier lifetime τ = 1 ns[1] and the illumination intensity used in our experiments (I = 6.5 mW cm^{-2}), we obtain n $\approx 3 \times 10^{-20}$ / f.u.

Given the similar values of the band gaps and the low estimated photocarrier density, at the illumination intensity used in our experiments and around room temperature, we may conclude that $|\Delta F^*| << |\Delta F^0(T)|$ for both $BZA_2PbBr_2I_2$ and $PEA_2PbBr_2I_2$, i.e., the tendency towards halide segregation is dominated by the compositional (in)stability of the considered systems, rather than a difference in the dynamical response of the systems to illumination.

Computational methods

We performed all calculations within density functional theory using the open-source Quantum ESPRESSO suite for quantum simulations of materials.[52,53] We employed the vdW-DF-cx density functional,[54–57] Garrity-Bennett-Rabe-Vanderbilt (GBRV) pseudopotentials,[58] a plane wave basis with a kinetic energy cutoff set to 60 Ry and a Monkhorst-Pack grid[59] with a 0.20 Å^{-1} k-point distance. The atomic positions and cell parameters were relaxed until the change in the total energy between two steps of ionic relaxation was less than 10^{-4} a.u. and the forces on all atoms were less than 10^{-3} a.u. The target pressure was set to 0 bar.

Preparation of perovskite thin films

Precursor solutions of 2D bromide/iodide perovskites A_2PbBr_4/I_4 were prepared by dissolving monovalent spacer salt (ABr/I) and lead halide ($PbBr_2/I_2$) with molar ratios of 2:1 in DMF solvent (DMF:DMSO=9:1 for HA_2PbBr_4, and DMF:GBL=85:15 for HA_2PbI_4 as exception), where A denotes different spacer cations. Precursor solutions of 2D mixed halide perovskites were prepared by dissolving spacer bromide salt (ABr), spacer iodide salt (AI), lead bromide ($PbBr_2$), and lead iodide (PbI_2) with molar ratios of 4:0:1:1 (for A_2PbBr_3I), 2:2:1:1 (for $A_2PbBr_2I_2$), and 0:4:1:1 (for A_2PbBrI_3) in DMF/DMSO solvent (See Table S1 for details). Quartz substrates were cleaned by ultrasonic with detergent, DI water, ethanol and IPA in sequence. O_2 plasma treatment (60 seconds) was employed to improve wetting. All perovskite thin films were deposited by spin-coating the precursor solution on a substrate at 4000 rpm for 30 s in an argon filled glovebox, followed by annealing at 100°C for 10 mins (for A_2PbBr_4/I_4 films). Annealing condition for $A_2PbBr_2I_2$ can be found in Table S1. The deposition conditions (solvents used, annealing temperature and time) for each spacer cation were carefully optimized to ensure that starting films exhibit high quality mixed halide phase, as determined from absorption and XRD measurements. The optimization target was to obtain a sharp single mixed phase peak in the absorption spectra, with the verification of the presence of single mixed phase by XRD measurements. Spin-coating speeds were 3000 rpm for thicker films for FTIR measurement. All precursor solutions were stirred overnight before use, and the concentration of Pb^{2+} was 0.2 M, except for FTIR samples, the concentration of Pb^{2+} was 0.4 M to get thicker films. For all compositions, solvent selection and annealing conditions were optimized to obtain high quality films based on absorption spectra and XRD patterns.

Thin film characterizations

Absorption spectra were measured with Agilent Cary 60 UV-Vis spectrometer. *In-situ* absorption spectrums were converted through Beer–Lambert law from transmittance spectrums (A =log(I_0/I), where I_0 and I were the light intensity before and after film absorption), which were recorded by a PDA-512 USB fiberoptic spectrometer (Control Development Inc.) under 100 mW cm^{-2} simulated solar illumination (Sunbrick^{TM} Solar Simulator, G2V) or 6.5 mW cm^{-2} white light source (150 W Xenon lamp) with an AM0 filter. Films for *in-situ* absorption measurements were encapsulated with a cover glass and ThreeBond TB3055B epoxy to avoid ambient exposure. XRD patterns of thin film were measured by Rigaku MiniFlex 600-C X-ray Diffractometer with Cu radiation source. FTIR spectra were obtained from Spectrum Two ATR-FTIR spectrometer (PerkinElmer). The structures shown in Figures S11 and S13 were confirmed by Rietveld refinement utilizing previously published structures. The periodicity (along the longest axis) was refined and amount to: 27.577(1) Å for BA_2BrBr_4 (according to Ref.[60]), 33.303(4) Å for BZA_2PbBr_4 (according to Ref.[61]), 17.577(4) Å for

PEA_2PbBr_4 (according to Ref.[61]), 33.497(1) Å for $(4FPEA)_2PbBr_4$ (according to Ref.[62]), 35.618 Å for HA_2PbBr_4 (calculated based on Ref.[63]), 31.356(2) Å for TEA_2PbBr_4 (according to Ref.[64]), 28.908(3) Å for TMA_2PbBr_4 (calculated based on Ref.[65]), 27.629(1)Å for BA_2BrI_4 (according to Ref.[66]), 28.743(1) Å for BZA_2PbI_4 (according to Ref.[67]), 32.871(1) Å for PEA_2PbI_4 (according to Ref.[61]), 16.731(7) Å for $(4FPEA)_2PbI_4$ (according to Ref.[68]), 35.618 Å for HA_2PbI_4 (according to Ref.[63]), 32.374(4) Å for TEA_2PbI_4 (calculated based on Ref.[64]), 28.908(3) Å for TMA_2PbI_4 (according to Ref.[65]), 27.498(2) for (i-BA) $_2PbBr_4$ (according to Ref.[69]) and 13.733(4) for $(i\text{-}BA)_2PbI_4$ (according to Ref.[70]).

To characterize Br:Pb and I:Pb ratios after illumination or bias, ITO/2PACz/2D perovskite/PCBM/BCP/Ag devices were prepared, where ITO denotes indium tin oxide coated glass substrates. 2PACz was spin-coated on ITO substrates at 4000 rpm for 30 s, followed by annealing at 100°C for 10 min. 2D perovskite films were then deposited as previously described. After cooling to room temperature (RT), PCBM layer was deposited on top of 2D perovskite by spin-coating PCBM in CB (20 mg/ml) solution with 1200 rpm for 30 s. After annealing at 100°C for 10 mins, BCP in IPA (0.5 mg/ml) was spin-coated on the top with 4000 rpm for 30 s. Then, the samples were transferred into a thermal evaporator for depositing 80 nm Ag. To evaluate effects of electrical bias up to 8 V (0-8 V, 0.3 V/s, double scan, ITO positive, Keithley 2400 Source Measure Unit) or 4 hours illumination under 1 Sun (Sunbrick^{TM} Solar Simulator, G2V), the Ag electrode was peeled off by a carbon tape. Then, 100 μl CB was dynamically spin-coated on the top of substrates at 5000 rpm for 30 s to remove PCBM layer. Br/Pb and I/Pb ratio were measured by energy dispersive X-ray spectroscopy (EDX) using Hitachi S4800 FEG SEM and Hitachi SU8230 FEG SEM with Oxford Ultim® Max detector (analysis area 170 mm^2). Samples for EDX measurements were not encapsulated, which ensures that stoichiometry changes, if any, would not be reversible due to the loss of volatile degradation products. Perovskite cross-section SEM images were measured using Hitachi S4800 FEG SEM. Photoluminescence (PL) spectrum was measured using XploRA Plus Raman/PL spectrometer with 405 nm excitation.